Elastic Scattering of 61.4-MeV Protons*

C. B. FULMER AND J. B. BALL
Oak Ridge National Laboratory, Oak Ridge, Tennessee 37830
AND
A. SCOTT† AND M. L. WHITEN‡
University of Georgia, Athens, Georgia
(Received 10 January 1969)

Proton elastic scattering angular distributions were measured for ^{12}C, ^{27}Al, ^{40}Ca, ^{58}Ni, ^{68}Zn, ^{90}Zr, ^{116}Sn, and ^{208}Pb with a 61.4-MeV beam from the Oak Ridge isochronous cyclotron. An optical-model analysis of the data was performed. The results show a nuclear symmetry dependence of the optical-model potential; this dependence can be related to either the real well depth or the radius parameter of the real well. This study, combined with previously reported studies at lower bombarding energies, shows that for targets of $A \geq 27$ a potential with fixed-geometry parameters and an energy-dependent real well depth,

$$-(V-0.4Z/A^{1/3}) \approx [49.9-0.215E+26.0(N-Z)/A] \text{ MeV},$$

will predict angular distributions in reasonable agreement with experiment for bombarding energies of 30–61 MeV. Data from light targets show a preference for large volume absorption and small surface absorption terms in the potential, while heavy-target data show a preference for small volume absorption and large surface absorption terms. The mean free path for a reaction of a 61-MeV proton in nuclear matter is estimated to be about $7\frac{1}{2}$ F.

I. INTRODUCTION

EXTENSIVE studies of proton elastic scattering have been reported for bombarding energies of 9–22,[1,2] 30,[3,4] and 40 MeV.[5,6] The principal interest in studies at additional bombarding energies is to better establish systematic trends in the optical-model potentials. The presence of a nuclear symmetry dependence of the optical-model potential was suggested by Green and Sood[7] and by Lane.[8] This dependence has been demonstrated several times to be consistent with the results of proton scattering in the energy range of 10–40 MeV.[9]

In the work reported here, elastic scattering data were obtained, at a bombarding energy of 61.4 MeV, for targets with a wide range of nuclear mass. Optical-model analyses of the data were performed. Preliminary results of this work, which were reported earlier,[10] showed the nuclear symmetry dependence of the potential that was observed at lower energies to be also consistent with the 61-MeV data. In the present report, data from a larger number of targets are included and the analyses are more extensive.

II. EXPERIMENTAL

A proton beam from the Oak Ridge isochronous cyclotron was magnetically analyzed to provide an energy spread of about 120 keV. For most of the data taken, this beam was transported 50 ft from the analyzing magnet with two triplet quadrupole magnets. The protons were focused to a $\frac{1}{8}$-in.-diam beam spot on the target, at the center of the scattering chamber, without the use of beam-defining collimators near the scattering chamber. Some data were obtained in another scattering chamber preceded by only one quadrupole magnet, but beam collimators used here had very little adverse effect.

The detector used in this experiment was a 1-in.-diam by $\frac{3}{4}$-in.-thick NaI(Tl) crystal, mounted on an RCA 6199 photomultiplier. Typical resolution varied from 0.9 to 1.1% for 61-MeV protons, depending on the over-all counting rate. The pulses from this detector were amplified by a Tennelec TC-200 amplifier and analyzed with a Victoreen 1600-channel analyzer. The collimator in front of the detector defined an angular acceptance of 0.6° for most of the data accumulated. Some data were obtained at large scattering angles with an angular acceptance of 0.8°, and some were taken at small angles with an angular acceptance of 0.4°. The angular position of the detector was indicated to

* Research sponsored by the U.S. Atomic Energy Commission under contract with the Union Carbide Corporation.
† Part of this work was completed while an Oak Ridge Associated Universities Summer Research Participant. Travel funds provided by Oak Ridge Associated Universities.
‡ Partial support from Office of General Research, University of Georgia. Travel funds from Oak Ridge Associated Universities.
[1] F. G. Perey, Phys. Rev. **131**, 745 (1963).
[2] L. Rosen, J. G. Berry, A. S. Goldhaber, and E. H. Auerbach, Ann. Phys. (N.Y.) **34**, 96 (1965).
[3] G. R. Satchler, Nucl. Phys. **A92**, 273 (1967).
[4] G. W. Greenlees and G. J. Pyle, Phys. Rev. **149**, 836 (1966).
[5] M. P. Fricke and G. R. Satchler, Phys. Rev. **139**, B567 (1965).
[6] M. P. Fricke, E. E. Gross, B. J. Morton, and A. Zucker, Phys. Rev. **156**, 1207 (1967).
[7] A. E. S. Green and P. C. Sood, Phys. Rev. **111**, 1147 (1958).
[8] A. M. Lane, in *Comptes Rendus du Congrès International de Physique Nucleaive; Interactions Nucleaives aux Basses Energies et Structure des Noyaux, Paris, 1958*, edited by P. Guggenberger (Dunod Cie., Paris, 1959), p. 32; Phys. Rev. Letters **8**, 171 (1962); Nucl. Phys. **35**, 676 (1962).
[9] P. E. Hodgson, in *Comptes Rendu du Congrès International de Physique Nucleaire, II, Paris, 1964*, edited by P. Gungenberger (Centre Nationale de la Recherche Scientifique, Paris, 1964), p. 258.
[10] C. B. Fulmer, J. B. Ball, A. Scott, and M. L. Whiten, Phys. Letters **24B**, 505 (1967).

TABLE I. List of targets.

Nucleus	Target material	Isotopic abundance	Thickness (mg/cm²)
^{12}C	Polystyrene	98.9%	2.3
^{27}Al	Metal	100%	3.0
^{40}Ca	Metal	96.8%	•••
^{58}Ni	Metal	99.95%	6.4
^{68}Zn	Metal	98.5%	4.9
^{90}Zr	Metal	98.6%	5.8
^{116}Sn	Metal	95.7%	5.1
^{208}Pb	Metal	99.3%	6.5

within 0.1°, and the zero angle checked by measuring the sharply falling differential cross section for ^{208}Pb at a number of scattering angles on either side of the beam axis.

All targets used, except ^{12}C, were rolled from isotopically enriched material into self-supporting metallic foils. The isotopic abundances and the thicknesses of these foils are shown in Table I. The ^{40}Ca target was accidentally destroyed before the thickness was determined, so the absolute magnitude of the differential cross section for this target is not well determined experimentally.

The targets chosen for this work span the periodic table and were selected from those having first excited states sufficiently far above the ground state that the inelastic peaks could be resolved from the elastic peak. Figure 1 shows representative pulse height spectra for protons scattered from ^{208}Pb. Low-mass contaminants had significant cross sections at some angles for this ^{208}Pb target, but even the worst case, at 28° which is

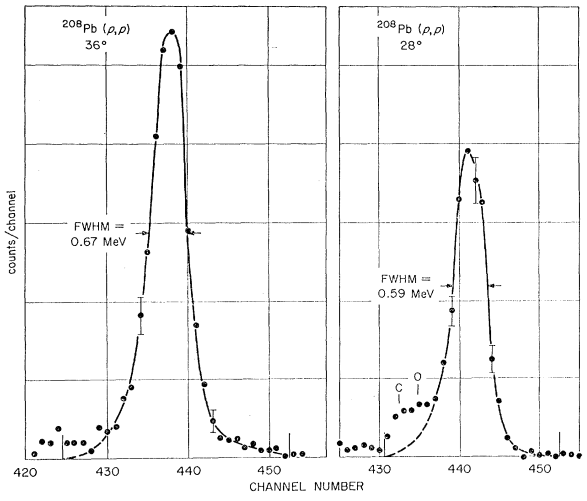

FIG. 1. Representative pulse-height spectra for ^{208}Pb. The elastic peaks deduced are the approximate Gaussians shown, with dashed low-energy tail. At 28° the target impurity peaks are more apparent than at 36°.

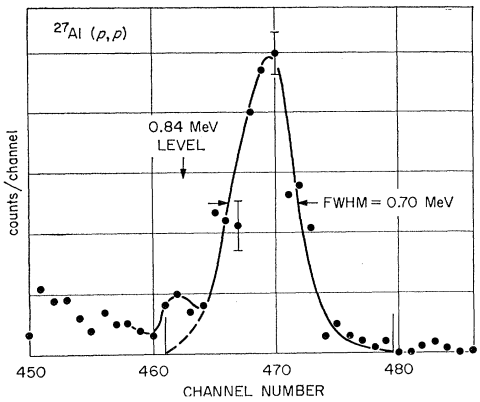

FIG. 2. Representative pulse-height spectrum for ^{27}Al at an angle where the inelastic scattering peak for the first excited state is largest relative to the elastic scattering peak. This level (at 0.84 MeV) is the lowest for any of the targets studied. The approximate Gaussian shown was used to obtain the elastic peak intensity.

shown in Fig. 1, presented no serious difficulty. The ^{27}Al nucleus has the lowest first excited state, at 0.84 MeV, and the peak associated with excitation of this state was observed on the low-energy tail of the elastic peak at some angles. This is illustrated in Fig. 2. Troublesome low-mass impurity peaks, particularly elastic scattering from oxygen, appeared at forward angles with the ^{40}Ca target and for this reason the cross sections for ^{40}Ca could not be extracted at angles less than 30°.

To determine the elastic peak intensities, the proton pulse height spectrum for each angle was plotted on log-linear graph paper and the counts totalled for the approximately Gaussian part of the elastic peak, as shown in Figs. 1 and 2. At those angles where a significant contaminant or inelastic peak appeared on the low-energy tail of the elastic peak, the Gaussian elastic peak shape from a nearby angle was used to extract the elastic peak intensity. A 5% correction was added to all elastic peak totals, as an estimate of the losses due to reactions in the crystal at 61-MeV proton energy.

Errors shown with the data include both the statistical error of the counts and an estimate of the uncertainty in determining the tail of the Gaussian elastic peak. The latter is significant where a contaminant peak or an inelastic peak is strongly excited. The uncertainty in the absolute value of the cross sections due to the determination of the effective target thickness is of order 5%, and the uncertainty in the charge collection measurements is about 10%.

III. EXPERIMENTAL RESULTS

Elastic scattering data from all targets included in this study are plotted as ratio-to-Rutherford in Fig. 3. The curves shown are optical-model predictions of the potentials obtained from the fixed-geometry optical-model searches which are discussed in Sec. IV. The data from all targets included in this work are presented in

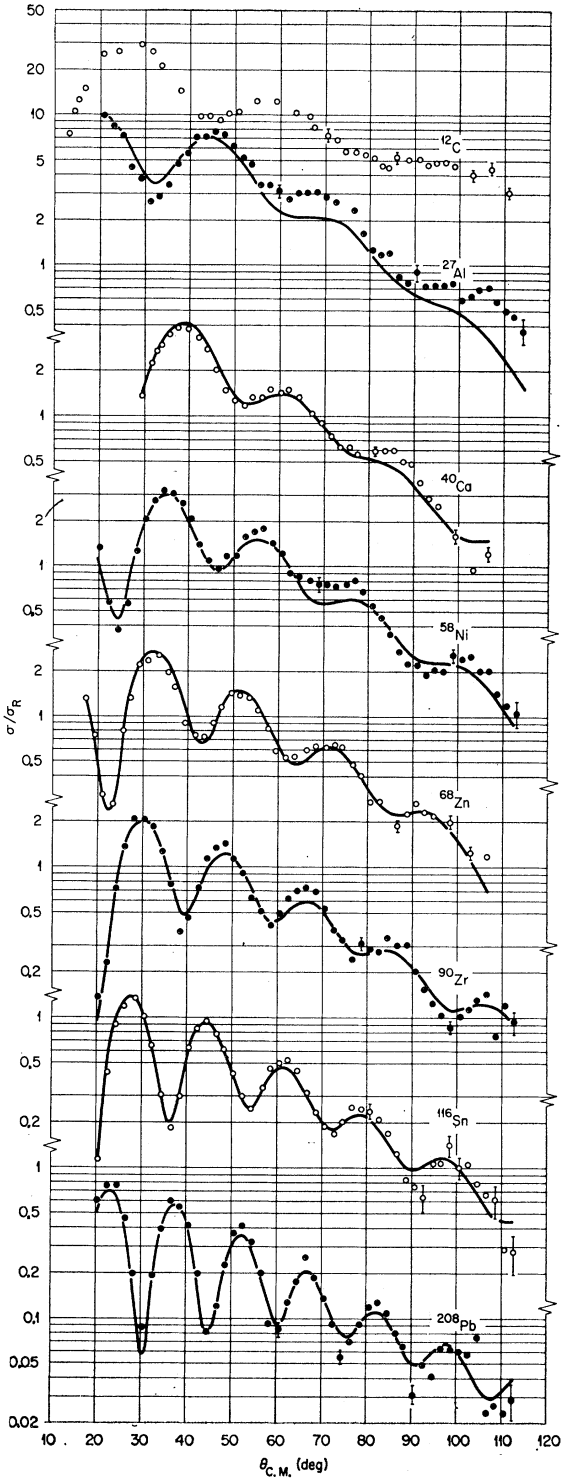

FIG. 3. Ratio-to-Rutherford angular distributions of 61.4-MeV elastic proton scattering from various nuclei. Typical statistical errors are shown for a few large-angle data points. At angles smaller than ~50° the statistical errors are smaller than the plotted points. The solid curves are optical-model predictions from the fixed-geometry searches.

tabular form in the Appendix. The errors shown include counting statistics and uncertainties in resolution of the elastic scattering peak.

In Fig. 4, the elastic scattering data from ^{27}Al, ^{58}Ni, ^{116}Sn, and ^{208}Pb are compared with optical-model predictions that were obtained from seven-parameter searches, which are described in the Sec. IV. The data for each target span about four orders of magnitude and, except for a few obviously poor data points, there is good agreement between the data and the optical-model predictions, both in the phases of the oscillations and the magnitude of the cross sections. The angular distributions from the optical-model calculations are

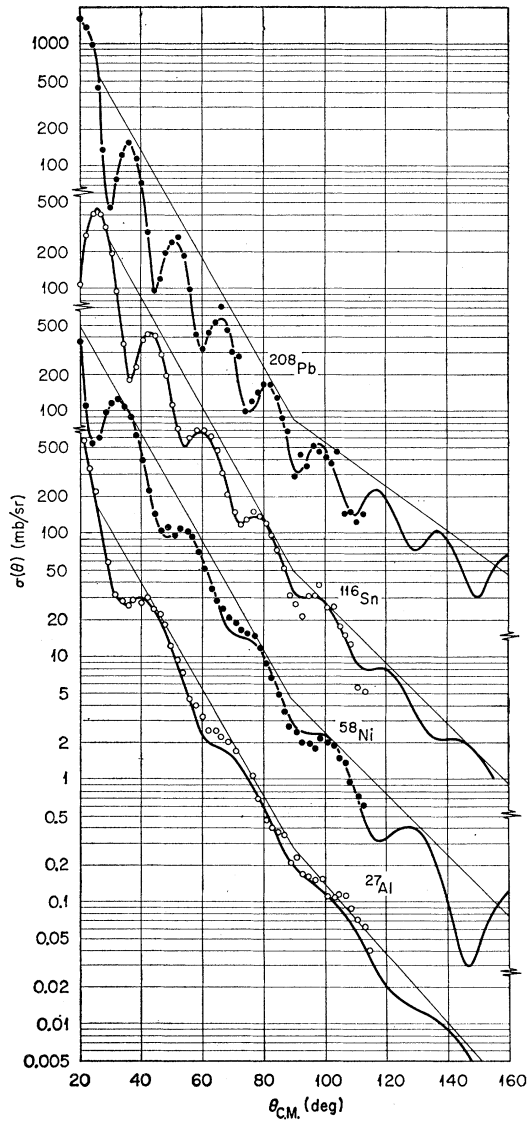

FIG. 4. 61.4-MeV proton elastic scattering angular distributions. The points are experimental data. The curves are optical-model results from the seven-parameter searches. The straight lines follow the envelopes of the angular distributions.

TABLE II. "Best-fit" optical-model parameters obtained from the seven-parameter searches. Spin-orbit parameters taken from Table II of Ref. 6 were used.

Target	V (MeV)	r_0 (F)	a (F)	W (MeV)	W_D (MeV)	r_0' (F)	a' (F)	σ_A (mb)	$\chi^2/(N-M)$
^{27}Al	36.78	1.174	0.660	6.36	0.333	1.45	0.629	545	2.3
^{58}Ni	41.11	1.160	0.728	6.66	2.324	1.33	0.504	891	2.2
^{68}Zn	38.27	1.208	0.750	8.57	2.281	1.24	0.773	1112	0.96
^{90}Zr	39.52	1.201	0.693	5.12	2.543	1.40	0.534	1239	2.1
^{116}Sn	41.93	1.197	0.687	3.80	5.014	1.24	0.808	1575	1.1
^{208}Pb	41.42	1.220	0.577	2.013	7.805	1.32	0.668	2162	1.8

extended to larger angles to indicate the predicted behavior of the data in that region.

Rost[11] has pointed out that a minimum at 90° in the envelope of the angular distribution of outgoing particles is characteristic of surface reactions that are localized to a very few partial waves. While such minima are not observed in the data shown in Fig. 4, there are perceptible changes in the slopes of the envelopes of the angular distributions predicted by the optical-model parameters which yielded the best fit to the data. This effect was also observed, and more pronounced, in 21-MeV α-scattering data reported earlier[12]; in those data there was a larger change in slope of the envelope of the inelastic scattering data than in the elastic scattering data. In the data of Fig. 4, the change of slope is most pronounced for ^{208}Pb and appears progressively smaller with decrease of target mass; for angles less than 90°, the envelopes of the angular distributions all have about the same slope.

As mentioned previously, the ^{40}Ca target was inadvertently destroyed after the data were obtained but before an accurate determination could be made of the target-foil thickness. Optical-model calculations showed the real well depth to be strongly dependent on the normalization of the cross sections, as illustrated in Fig. 5. The absolute normalization of the ^{40}Ca data was assigned as follows: The fixed-geometry optical-model parameter searches (described in Sec. IV) with the data obtained from other even-A targets yielded values of the real well depth, that, with conventional Coulomb corrections,[1] show a linear dependence of the real well depth on the nuclear symmetry parameter, $(N-Z)/A$. The normalization of the ^{40}Ca data was varied until a fixed-geometry search yielded a value of V that matches the straight line fit to values of V obtained from the other even-A targets.

IV. OPTICAL-MODEL ANALYSIS

Optical-model calculations were performed with the ORNL automatic search computer code HUNTER,[13] which minimizes the quantity

$$\chi^2=\sum_i\{[\sigma_{\mathrm{TH}}(\theta_i)-\sigma_{\mathrm{EX}}(\theta_i)]/\Delta\sigma_{\mathrm{EX}}(\theta_i)\}^2.$$

The calculations used a local potential of the usual form

$$U(r)=-V(e^x+1)^{-1}-i(W-4W_Dd/dx')(e^{x'}+1)^{-1}+(\hbar/m_\pi c)^2V_s(\boldsymbol{\sigma}\cdot\mathbf{L})r^{-1}(d/dr)(e^{x_s}+1)^{-1},$$

where

$$x=(r-r_0A^{1/3})/a,$$
$$x'=(r-r_0'A^{1/3})/a',$$
$$x_s=(r-r_sA^{1/3})/a_s.$$

The notation for the parameters is the same as that of Ref. 3. To $U(r)$ is added the Coulomb potential from a uniformly charged sphere of radius $1.25A^{1/3}$ F.

The proton energy in this work is sufficiently high that one should not ignore relativistic effects. It has been pointed out[14,15] that the nonrelativistic procedure is valid if the correct relativistic wave number is obtained by using an effective laboratory energy with nonrelativistic conversion from laboratory to c.m. system. In the present work, this would mean the calculations should be done by increasing the laboratory bombarding energy by amounts ranging from 1.4 MeV for ^{12}C to 2.0 MeV for ^{208}Pb. This was done for ^{208}Pb in one case. A sequence of searches, referred to below as "seven-parameter searches," was done for the ^{208}Pb data with and without the adjustment in bombarding energy. There were small differences in the final values of the parameters and the final values of χ^2 were 84 and 70, respectively, for the searches with and without the adjustment in bombarding energy. In as much as the differences are small, and since one application of the results of the analyses may be for use as proton parameters in distorted wave calculations for inelastic scattering and transfer reactions, the results of the optical-model analyses reported here are for calculations in which adjustments were not made in the bombarding energy.

[11] E. Rost, Phys. Rev. **128**, 2708 (1962).
[12] C. B. Fulmer, J. Benveniste, and A. C. Mitchell, Phys. Rev. **165**, 1278 (1968).
[13] R. M. Drisko, Oak Ridge National Laboratory (unpublished).
[14] G. R. Satchler, Nucl. Phys. **A100**, 497 (1967).
[15] L. R. B. Elton, Nuovo Cimento **43**, 277 (1966).

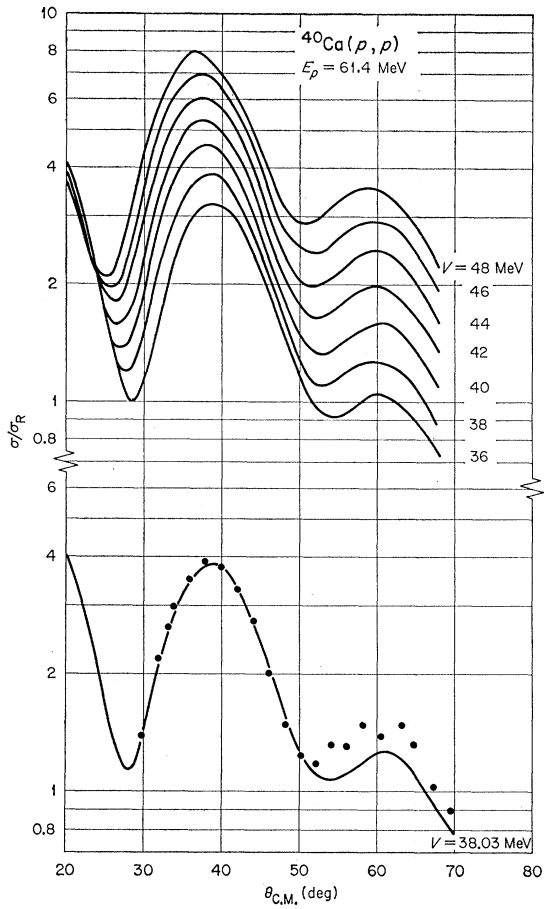

FIG. 5. Normalization of the angular distributions for 61.4-MeV proton elastic scattering from ^{40}Ca as a function of the real well depth V. In the lower part of the figure, the experimental data are compared with an angular distribution obtained from the fixed-geometry search which yielded the desired value of V.

For initial values of the parameters we used the results of the 40-MeV work of Fricke *et al.*[6] Since 61.4-MeV polarization data are not available, the spin-orbit parameters, V_s, r_s, and a_s, were not varied in the present work. The variable parameters are the real well depth V, the radius parameter of the real well r_0, the diffuseness of the real well a, the volume imaginary well depth W, the surface imaginary well depth W_D, the radius parameter of the imaginary well r_0', and the diffuseness of the imaginary well a'.

The data were analyzed with four different search sequences. These were (1) seven-parameter, (2) fixed-geometry, (3) W-grid, and (4) fixed-geometry W-grid. The ^{12}C data and analysis are discussed in a separate section.

A. Seven-Parameter Searches

In these searches, the real and imaginary well depths and the geometrical parameters for these wells were allowed to vary. The sequences of parameter searches was r_0; a, r_0', a'; V, W_D; V, W; and finally V, W, W_D, r_0, a, r_0', a'. Each search after the first used the results of the preceding one. The final parameters obtained from these searches are listed in Table II along with the σ_A (total reaction cross section) and $\chi^2/(N-M)$ values, where N is the number of data points and M is the number of variable parameters.

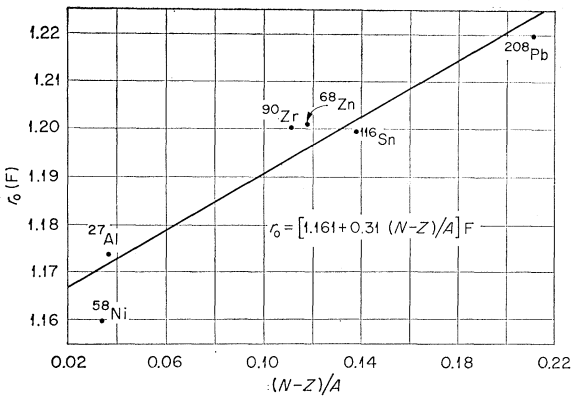

FIG. 6. Values of r_0, obtained from the seven-parameter searches, versus $(N-Z)/A$. The straight line is a least-squares fit to the points.

In Fig. 4, the experimental data from four of the targets are compared with optical-model predictions of potentials with the final parameters obtained in the seven-parameter searches. The comparisons for other targets are of similar quality. In general, the agreement is reasonable both in the phases of the oscillations and in the magnitude of the cross sections. The optical-model calculation for ^{58}Ni shows a minimum near 70° that is more pronounced than the data. This was observed in all reasonable fits to the ^{58}Ni data. The ^{58}Ni data in this angular region were repeated in a subsequent data run; the two sets of experimental data are in good agreement.

The imaginary well depth parameters listed in Table II show a hint of a systematic pattern. The analyses of the light-target data yielded large volume absorption terms and small surface absorption terms. As the target mass is increased the volume absorption becomes

TABLE III. Optical-model parameters obtained from fixed-geometry searches. For these searches the fixed parameters were $r_0 = 1.16$ F, $a = 0.75$ F, $r_0' = 1.37$ F, $a' = 0.63$ F, $V_s = 6.04$ MeV, $r_s = 1.064$ F, $a_s = 0.738$ F.

Target	V (MeV)	W (MeV)	W_D (MeV)	σ_A (mb)	$\chi^2/(N-M)$
^{27}Al	37.96	4.81	1.634	533	7.9
^{40}Ca	38.03	1.45	4.44	744	7.6
^{58}Ni	40.29	6.83	0.834	908	3.6
^{68}Zn	42.51	7.99	1.39	1122	4.4
^{90}Zr	42.86	4.66	3.99	1279	4.2
^{116}Sn	44.18	4.76	3.90	1565	1.5
^{208}Pb	47.12	5.98	4.15	2136	7.8

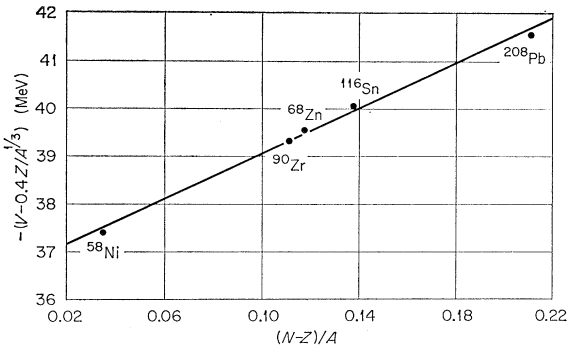

FIG. 7. Values of the real well depth minus Coulomb correction versus $(N-Z)/A$. The values of V were obtained from the fixed-geometry searches. The straight line is a least-squares fit to the points.

smaller and the surface absorption increases. (The ^{68}Zn data depart slightly from this pattern with a large value of the volume absorption well depth.) This behavior of the parameters obtained from the analyses is consistent with the changes of slopes of the envelopes of the angular distributions. The heavy targets show a stronger characteristic of surface reactions by more pronounced change of slope of the envelopes.

It is well known that the phase of the oscillations in the angular distributions is determined principally by VR_0^n, where $R_0=r_0A^{1/3}$ and $n\sim2$–3. The sequence of parameter searches resulted in adjustments in r_0 for the initial fitting. This adjustment in r_0 resulted in a relatively small spread in real well depth values.

The nuclear symmetry dependence of the optical-model potential has usually been ascribed to the real well depth. It has recently been pointed out[3] that, if the symmetry dependence of the potential is assumed to be responsible for (p, n) reactions observed between analog states, it could be interpreted as a nuclear symmetry dependence of the radius parameter for the real well depth. In Fig. 6, the values of r_0, listed in Table II, are plotted as a function of $(N-Z)/A$. A straight-line least-squares fit to the plot yields a value of 0.31 F for the coefficient of $(N-Z)/A$. This is in reasonable agreement with the value of 0.25 F obtained from the 30-MeV proton scattering results[3] and the value of $\sim$0.3 F from the analysis of (p, n) reactions by Satchler, Drisko, and Bassel.[16]

B. Fixed-Geometry Searches

For these searches the average-geometry parameters obtained in the 40-MeV work of Fricke *et al.*[6] were used as fixed-geometry parameters and χ^2 was minimized by varying the real and imaginary well depths only. The geometrical parameters that were used and the well depths that were obtained from these searches are given in Table III; values of $\chi^2/(N-M)$ and total reaction cross sections are also tabulated.

Since the phase of the oscillations of elastic scattering angular distributions is determined largely by VR_0^n, the results of the fixed-geometry searches should test the data for evidence of a nuclear symmetry dependence of the real well depth. The values of V (with conventional[1] Coulomb corrections) listed in Table III for the even-even targets are plotted in Fig. 7 as a function of $(N-Z)/A$. A straight-line least-squares fit yields a nuclear symmetry parameter of 23.6 MeV. In Ref. 10, a value of 27.2 MeV was quoted for the nuclear symmetry parameter. In that work a target thickness error for the ^{116}Sn target resulted in an absolute normalization of the cross sections that was 30% too large. As in the case of ^{40}Ca, a too large normalization of the cross sections results in a too large value of the real well depth from the fixed-geometry searches. The value of 23.6 MeV is obtained for the nuclear symmetry parameter when the ^{116}Sn data are corrected and the ^{68}Zn data are included in the straight-line least-squares fit. The change in real well depth associated with the 30% correction to the ^{116}Sn data was 1.5 MeV. This implies errors due to absolute normalization uncertainties to be of order 0.5 MeV for the values shown in Fig. 7.

When the data at angles $\leq60°$ for ^{40}Ca and ^{68}Zn were obtained there were corrections of 1° to the angles due to an off-set of the scattering chamber axis with respect to the incident proton beam. The optical-model searches on the ^{68}Zn data were begun inadvertently without this correction; the angles for the data points forward of 60°

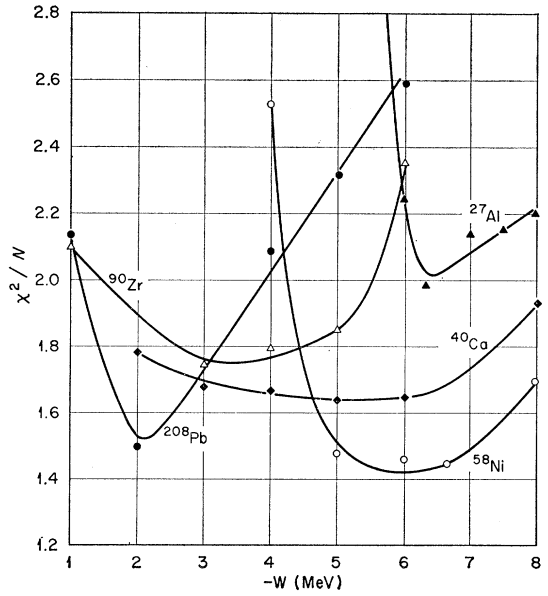

FIG. 8. Values of χ^2/N versus W. The plotted points were obtained from the six-parameter W-grid searches. Curves are drawn to indicate the trend of the results.

[16] G. R. Satchler, R. M. Drisko, and R. H. Bassel, Phys. Rev. **136**, B637 (1964).

being 1° too large. The value of V thus obtained from the fixed-geometry search was 39.2 MeV, or 3.3 MeV smaller than the value listed in Table III. This demonstrates that the results of 61-MeV optical-model analyses, especially for V or r_0, are moderately sensitive to the phases of the oscillations in the angular distributions.

For all of the targets the value of $-(V-0.4Z/A^{1/3})$ plotted in Fig. 7 fall very close to the straight-line fit. This suggests that the errors are small for both the determination of the angles and the absolute normalization of the cross sections. There is a possibility that the departures of individual points from the straight-line fits are fortuitously small. In the analysis of 11-MeV proton scattering data from targets in the mass region between ^{48}Ti and ^{76}Ge, Perey and Perey[17] observed the real well depth to decrease with increase of $(N-Z)/A$ for targets of the same isotopic spin. All of the targets represented by the points plotted in Fig. 7 have different isotopic spins. The only targets used in this work with the same isotopic spins are ^{12}C and ^{40}Ca (both have $T=0$). We thus did not obtain any information about the nuclear symmetry dependence of the real well depth for targets of the same isotopic spin.

Fricke *et al.*[6] used the 40-MeV average-geometry parameters to obtain reasonably good fits to the 30-MeV proton scattering data of Ridley *et al.*,[18] Craig *et al.*,[19] and Turner *et al.*[20] and deduced that the energy dependence of the real well depth in the energy range 30–40 MeV is

$$dV/dE=-0.22\pm0.03,$$

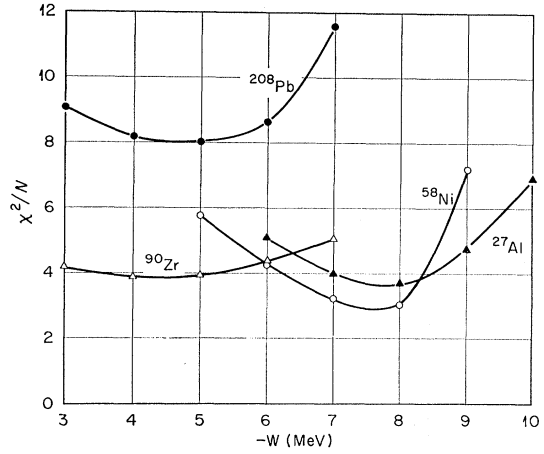

FIG. 9. Values of χ^2/N versus W. The plotted points were obtained from the fixed-geometry W-grid searches. Curves are drawn to indicate the trend of the results.

[17] C. M. Perey and F. G. Perey, Phys. Letters **26B**, 123 (1968).
[18] B. W. Ridley and J. F. Turner, Nucl. Phys. **58**, 497 (1964).
[19] R. M. Craig, J. C. Dore, G. W. Greenlees, J. S. Lilley, J. Lowe, and P. C. Rowe, Nucl. Phys. **58**, 515 (1964).
[20] J. F. Turner, B. W. Ridley, P. F. Cavanagh, G. A. Gard, and A. V. Hardacre, Nucl. Phys. **58**, 509 (1964).

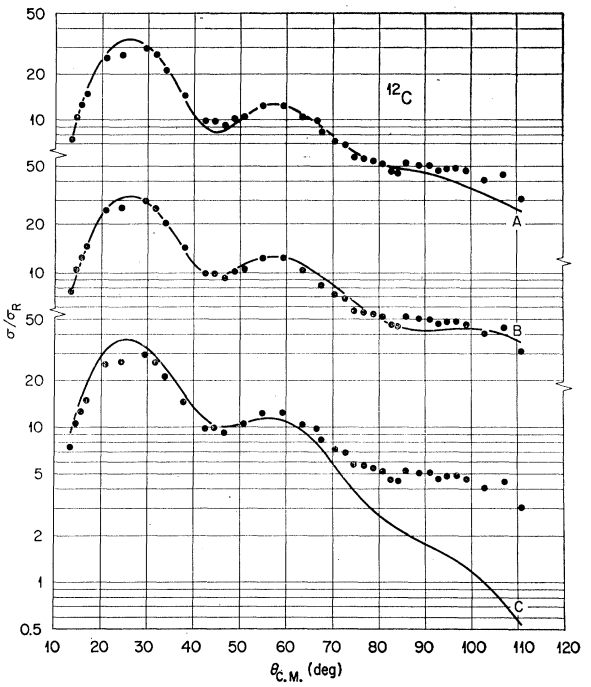

FIG. 10. 61.4-MeV proton elastic scattering angular distributions for ^{12}C. The points are experimental data. The curves are optical-model predictions from searches A, B, and C. The searches are described in the text.

where E is the proton energy in MeV. The real well depth for 40-MeV protons is described by

$$-(V-0.4Z/A^{1/3})=[41.4+26.4(N-Z)/A]\text{ MeV}.$$

In the 61.4-MeV work reported here, optical-model searches with the same geometry parameters yielded a real well depth described by

$$-(V-0.4Z/A^{1/3})=[36.7+23.6(N-Z)/A]\text{ MeV}.$$

These results imply the energy dependence of V in the energy range 40–61 MeV to be

$$dV/dE=-0.21,$$

in good agreement with the value obtained by the authors in Ref. 6 in the energy range 30–40 MeV.

C. Six-Parameter W-Grid Searches

The pattern of the imaginary well depth parameters obtained from the seven-parameter searches suggested that a more extensive investigation of the volume absorption term of the optical-model potential might be useful. An investigation of this type was made as follows. A value of the volume absorption term W was assigned. Starting values for the other parameters were those used in the fixed-geometry searches. The search

TABLE IV. Optical-model potential parameters for ^{12}C. The absorption in A is all surface; the absorption in B is all volume. The geometrical parameters in C are fixed; they are the same as the fixed-geometry parameters in Table III.

Potential	V (MeV)	r_0 (F)	a (F)	W (MeV)	W_D (MeV)	r_0' (F)	a' (F)	σ_A (mb)	$\chi^2/(N-M)$
A	20.7	1.44	0.60	0	3.45	1.03	0.48	141	2.69
B	19.2	1.48	0.61	2.78	0	1.45	0.06	111	1.63
C	33.8	1.16	0.75	2.95	1.37	1.37	0.63	243	25.6

sequence was V, W_D; V, r_0', W_D; V, r_0', a', W_D; V, r_0, a, r_0', a', W_D. As in the seven-parameter searches each search after the first used the results of the preceding one. After completion of the sequence a new value of W was assigned and the search sequence was repeated with the original starting value of the other parameters. Thus a plot of χ^2 versus W was obtained for each target.

Plots of (χ^2/N) versus W are shown in Fig. 8 for several targets. Because of the relatively large amount of computer time needed for these searches W-griding was not done for all targets. Except for ^{40}Ca the plot of each curve in Fig. 8 exhibits a reasonably well defined minimum. The value of W, at which the minimum occurs, decreases as the mass of the target nucleus increases. The surface absorption term W_D decreased smoothly with increase of W for all targets. As would be expected from the search sequence used, the radius parameter for the real well was almost constant for each element for all of the values of W included in the searches. The radius parameter for the imaginary wells all increased with W. There were some fluctuations in the diffuseness parameters as W was varied.

The results of the W-grid searches appear to support the trend observed in the seven-parameter searches, i.e., the volume absorption is large for light targets and the surface absorption is small; as the target mass increases the surface absorption term becomes larger with a corresponding decrease in the volume absorption term. This is also consistent with the behavior of the envelopes of the angular distributions that was discussed above.

D. Fixed-Geometry W-Grid Searches

To remove possible effects of variations of the geometrical parameters on the results, W-grid searches with fixed-geometry parameters were done for four targets. The values of the fixed-geometry parameters are the same as those used in the 61-MeV fixed-geometry optical-model searches discussed above. In these searches a value of W was assigned and the search sequence V; V, W_D was made. Then a new value of W was assigned and the search sequence was repeated.

The plots of (χ^2/N) versus W obtained from these searches are shown in Fig. 9. With only two adjustable parameters, χ^2 values are appreciably larger than those obtained for the W-grid searches in which there were six adjustable parameters. The trend is less pronounced than in the case of the six-parameter W-grid searches but the results are qualitatively the same; the preferred value of the volume absorption term of the optical-model potential decreases with increasing target mass. The largest change is observed for ^{208}Pb; the χ^2 is much larger, the minimum is less well defined, and it occurs at a larger value of W. The minimum in the plot for ^{90}Zr is also poorly defined.

E. Analysis of ^{12}C

The principal interest in including ^{12}C in this survey of elastic scattering is that a number of studies at lower

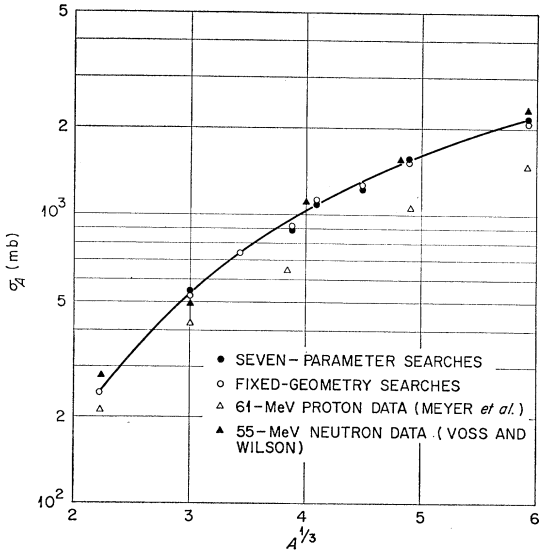

FIG. 11. Reaction cross sections versus $A^{1/3}$. The circular points were obtained from optical-model calculations for 61.4-MeV proton elastic scattering data. The curve is drawn through these points to indicate the trend. Experimental measurements for 61-MeV protons and 55-MeV neutrons are also shown.

bombarding energies have been reported.[14,21,22] Optical-model analyses of carbon data at lower energies have encountered difficulties. In the recent work of Satchler[14] at 46 MeV, both elastic cross sections and polarization measurements were available; it was possible to find good fits to both sets of data separately but not simultaneously.

In the present work only elastic scattering cross sections were measured. A number of optical-model analyses were made. Some of these yielded good fits to the data but the parameters had unreasonable values. The best fits, in terms of χ^2, tended toward real well depths of less than 20 MeV. In some cases the absorption terms of the potential became very large, with one term positive and the other negative.

In Fig. 10, angular distributions predicted by the results of three searches are compared with the data. These illustrate the results and difficulties of the somewhat more extensive analysis. The parameters obtained from these searches, values of $\chi^2/(N-M)$, and the σ_A values are listed in Table IV. The three searches include (A) the imaginary potential is all surface absorption; (B) the imaginary potential is all volume absorption; and (C) the geometrical parameters are fixed. The geometry parameters for the latter search are the average-geometry parameters of the 40-MeV work of Fricke *et al.*[6]

In terms of χ^2, potential B yielded the best fit but there is not an obvious choice between A and B. The diffuseness term for the imaginary well for potential B is surprisingly small. Both A and B potentials have rather low values of the real well depth and reaction cross sections.

Potential C predicts an angular distribution that is in reasonable agreement with the data for angles $\lesssim 70°$. At larger angles there are large discrepancies between the data and the optical-model predictions; 73% of the χ^2 obtained in this fixed-geometry search is due to angles larger than 70°.

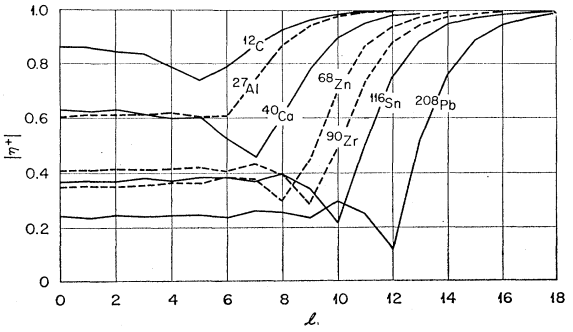

FIG. 12. Values of the reflection coefficient $|\eta_l|$ versus orbital angular momentum. These values were obtained from the fixed-geometry searches.

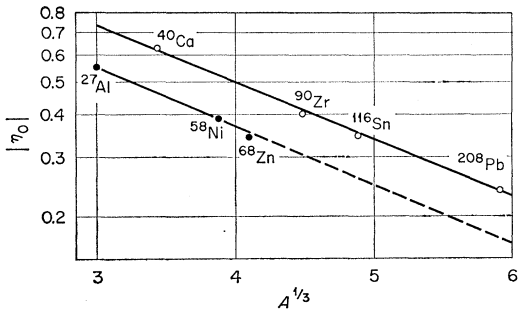

FIG. 13. Plot of reflection coefficients for $l=0$ versus $A^{1/3}$. These values were obtained from the fixed-geometry searches. Either curve is described by $|\eta_0| \propto \exp(-0.4A^{1/3})$.

The value of σ_A obtained in the fixed-geometry search agrees reasonably well with an extrapolation from values in the fixed-geometry fitting of data from targets of larger mass (see Fig. 11). The value of V is a little low when compared with the other values obtained from such searches but not nearly so low as is obtained for potentials A and B where the geometry parameters are not fixed.

The principal difficulty with potential C is that it does not fit the data at large angles. Potential A and B fit the large-angle data reasonably well; these searches yielded rather large values of r_0 and small values of V. The combinations predict angular distributions that also fit the forward angle data. The positions of maxima and minima are dependent on VR^n, hence a small value of V would require a large value of r_0 to obtain phase agreement with experimental angular distribution data.

While fixed-geometry searches for heavier targets do not yield as good fits as the seven-parameter searches, the parameters, σ_A values, and fits for the entire angular distributions are reasonable. Consistent optical-model potentials can be found for targets of mass $\gtrsim 27$ and for bombarding energies ranging from 30 to 61 MeV with the average geometry parameters. This is also valid for the 61-MeV carbon data for angles below $\sim 70°$. The 61-MeV data from carbon at large angles are not in good agreement with a potential obtained from the fixed-geometry parameter searches.

V. DISCUSSION

The results of the fixed-geometry searches demonstrate that the 40-MeV parameters of Fricke *et al.*[6] can be used to define an optical-model potential which predicts elastic scattering angular distributions that agree reasonably well with experimental measurements for targets of $A \gtrsim 27$ and for bombarding energies of 30 to 61 MeV. By comparing the results of the present

[21] L. N. Blumberg, E. E. Gross, A. Van der Woude, A. Zucker, and R. H. Bassel, Phys. Rev. **147**, 812 (1966).
[22] R. M. Craig, J. C. Dore, G. W. Greenlees, J. Lowe, and D. L. Watson, Nucl. Phys. **83**, 493 (1966).

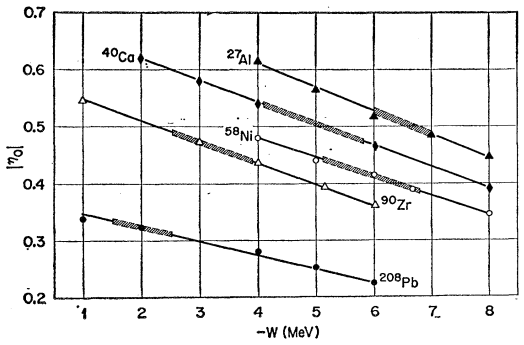

FIG. 14. Plots of $|\eta_0|$ versus W. The values of $|\eta_0|$ were obtained from the six-parameter W-grid searches. The minima in the corresponding curves of Fig. 8 are in the interval of W indicated by the thick portion of the line. The corresponding ordinate values are considered the limits of uncertainty of $|\eta_0|$ values.

study with those of Ref. 6 one may express the real well depth of the average-geometry potential,

$$-(V-0.4Z/A^{1/3}) \approx[49.9-0.215E+26.0(N-Z)/A]\ \text{MeV}.$$

The absorption terms of the potential are not so well defined for the range of bombarding energies. The fixed-geometry W-grid searches of the present work (see Fig. 9) indicate that a potential with a volume absorption term of $-W=6.0$ MeV and a surface absorption term given by

$$-W_D=(1.28A^{1/3}-3.5)\ \text{MeV}$$

would yield angular distributions in reasonable agreement with experimental measurements. Since W-grid calculations are not available for the data at lower bombarding energies, possible energy dependence of the absorption terms cannot be deduced from the present study.

The reaction cross sections listed in Tables I and II are plotted as a function of $A^{1/3}$ in Fig. 11. The values for each target obtained in the fixed-geometry searches and the seven-parameter searches are in good agreement with each other. The values of σ_A obtained for the sets of parameters that yielded values of χ^2 near the minima of the plots in Figs. 8 and 9 are also in good agreement with the corresponding values plotted in Fig. 11. A smooth curve readily fits the reaction cross sections obtained in this work, as shown in Fig. 11. A puzzling result is that the values of σ_A thus obtained are somewhat larger than the experimentally measured total reaction cross sections for 61-MeV protons.[23] The latter are plotted in Fig. 11 for comparison with the values obtained in the present work. The disagreement between the experimentally measured values of σ_A and the values obtained from optical-model analysis of 61.4-MeV proton elastic scattering data is in contrast to the good agreement reported in Ref. 6 between values of σ_A obtained from 30-MeV optical-model fits and 28.5-MeV reaction cross section measurements.[20] Observed values of σ_A for 55-MeV neutrons[24] are also plotted in Fig. 11. The agreement between these data and the present results is much better than either with the 61-MeV proton measurements of Ref. 23.

The authors of Ref. 6 investigated the behavior of the

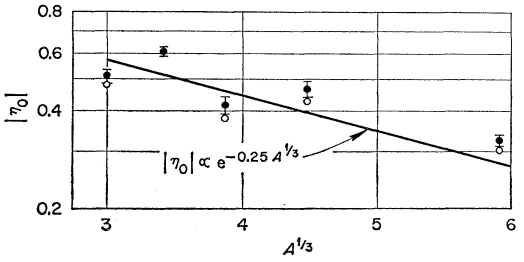

FIG. 15. Plots of reflection coefficients for $l=0$ versus $A^{1/3}$. Points shown by full circles were obtained from the six-parameter W-grid searches; points shown by open circles were obtained from the fixed-geometry W-grid searches.

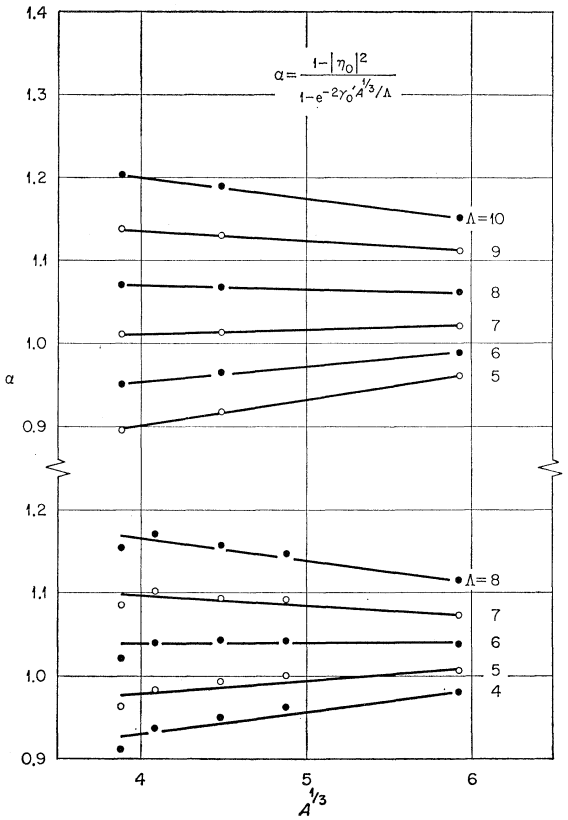

FIG. 16. Plots of α versus $A^{1/3}$ for various values of Λ. The value of Λ that yields a constant value of α corresponds to the mean free path for a reaction in nuclear matter. The upper family of curves corresponds to the values of $|\eta_0|$ shown in Fig. 15. The lower set corresponds to the values of $|\eta_0|$ from Fig. 13 for the non-closed-shell nuclei.

[23] V. Meyer, R. M. Eisberg, and R. F. Carlson, Phys. Rev. **117**, 1334 (1960).

[24] R. Voss and R. Wilson, Proc. Roy. Soc. (London) **A236**, 41 (1958).

reflection coefficients $|\eta_l|$ obtained in their 40-MeV optical-model studies. The values of $|\eta_0|$ were used to determine a value of $\Lambda=7$ F for the mean free path for a reaction of a 40-MeV proton in nuclear matter. In that work, plots of $|\eta_l|$ versus orbital angular momentum were fairly flat for small values of l, dipped sharply for a value of l close to the nuclear surface, and then rose sharply to 1.0 for larger values of l. Plots of $|\eta_l|$ versus l obtained from the fixed-geometry searches in the present work are shown in Fig. 12. These plots are also rather smooth for small values of l, and for targets heavier than ^{27}Al there is a dip at a value of l near the nuclear surface. The dips are not as deep, however, as those observed in the 40-MeV work of Ref. 6. The values of $|\eta_0|$ decrease with increasing mass of the target nucleus but not monotonically as was observed in Ref. 6.

The values of $|\eta_0|$ obtained from the fixed-geometry searches are plotted as a function of $A^{1/3}$ in Fig. 13. As in Ref. 6, it is observed that $|\eta_0|$ is an exponential function of the nuclear radius. In contrast to the 40-MeV results where all of the points fall close to the same straight line on the plot, there appear to be two groups of points in Fig. 13; each group falls on a straight line and both lines have about the same slope. Either line can be represented by $|\eta_0| \propto \exp(-0.4A^{1/3})$. The ordinate values of the upper curve are almost 50% larger than the corresponding values on the lower curve. It is noted that each point on the upper curve was obtained for a target with a major closed shell for protons, neutrons, or both, while the targets corresponding to the plotted points on the lower curve do not contain closed nucleon shells (a possible exception is ^{58}Ni with the weakly closed proton shell at $Z=28$). The larger values of $|\eta_0|$ obtained for the closed-shell nuclei indicate a lower probability of an $l=0$ proton undergoing a nuclear reaction while traversing a closed-shell nucleus. Such a result seems consistent with the sharp decrease in number of possible interactions with the closed configurations as a result of the exclusion principle.

We explored the possibility that the parameters used in the fixed-geometry searches might be influencing the values of $|\eta_0|$ obtained in the optical-model calculations. The values of $|\eta_0|$ obtained in the six-parameter W-grid searches are plotted as a function of W in Fig. 14. In each case the reflection coefficient decreases with increase of the volume absorption term. The thick portions of the curves of Fig. 14 represent our estimates for limits of the abscissa values defining the minima of the curves in Fig. 8. The corresponding ranges of values of $|\eta_0|$ are plotted as full circles in Fig. 15. Values of $|\eta_0|$ obtained in a similar manner from the fixed-geometry W-grid searches are plotted as open circles in Fig. 15. In each case the $|\eta_0|$ values for closed-shell nuclei are larger than the corresponding values for target nuclei that do not have strongly closed nucleon shells.

The authors of Ref. 6 obtained a correlation between $|\eta_0|$ and Λ, the mean free path for a reaction in nuclear matter. We have used the same method to obtain estimates of Λ from the present work. For $l=0$ protons the path length in nuclear matter is assumed to be $\sim 2r_0'A^{1/3}$, and the probability of a reaction is $[1-\exp(-2r_0'A^{1/3}/\Lambda)]$. Thus,

$$1-\eta_0^2=\alpha[1-\exp(-2r_0'A^{1/3}/\Lambda)]$$

is expected to be a constant for all nuclei whose diameters are large compared to the proton mean free path. Plots of α versus $A^{1/3}$ for several values of Λ for targets of mass ≥ 58 are shown in Fig. 16. The η_0 values used to compute the two sets of values of α were taken from the plots of Figs. 13 and 15. The value of Λ obtained from the average curve shown in Fig. 15 is about $7\frac{1}{2}$ F, with a value of $\alpha\sim 1.04$. This compares reasonably well with the value of $\Lambda=7$ F and $\alpha=1.1$ obtained in the 40-MeV work of Fricke *et al.*[6] The value of Λ obtained from the lower curve of Fig. 13 is about 6 F and from the upper curve is about 10 F. This difference may possibly be due to closed-shell effects as discussed previously. Again, if an average curve is assumed, as in Fig. 15, the deduced value of Λ would be about $7\frac{1}{2}$ F.

The analysis of the present experiment was made in terms of the conventional optical model. No attempt was made to treat the data in terms of recently suggested modifications to these procedures.[25,26] Although such an analysis would be interesting, it was deemed outside the scope of the present paper.

ACKNOWLEDGMENTS

The authors wish to thank T. H. Jeong, D. P. Cauffman, Mavis George Cauffman, and A. E. Pugh for assistance during the initial phases of this work. Our thanks also go to G. R. Satchler for valuable discussions concerning the optical-model calculations. We are indebted to the operating crew of ORIC for their efforts in providing the 61-MeV proton beam.

APPENDIX

Since a preliminary report of this work was published,[10] a number of people have requested the cross-section data. We are therefore presenting the data in tabular form below in Tables V–XII. The errors shown are based on counting statistics and uncertainties in the subtraction of contaminant or inelastic peaks. Target thickness and beam monitoring uncertainties could contribute as much as 10% error to the absolute cross sections. The normalization of the ^{40}Ca cross sections is based on fixed-geometry optical-model calculations, as described in Sec. III.

---

[25] G. W. Greenlees, G. J. Pyle, and Y. C. Tang, Phys. Rev. **171**, 1115 (1968).

[26] N. Berovic, P. M. Rolph, and S. M. Scarrott, Phys. Letters **27B**, 477 (1968).

TABLE V. Differential cross sections for elastic scattering of 61.4-MeV protons on ^{12}C.

$\theta_{c.m.}$ (deg)	$\sigma(\theta)$ (mb/sr)	±%
13.0	656	5
14.1	665	5
15.2	601	5
16.2	550	5
20.6	364	5
24.0	206	5
29.2	106	5
31.4	72.7	5
33.5	45.3	5
37.8	19.4	5
42.1	8.62	5
44.2	7.11	5
46.3	5.67	5
48.5	5.24	5
50.6	4.64	5
54.8	4.02	5
59.0	3.02	5
63.2	2.01	5
66.2	1.62	5
67.3	1.32	5
70.4	0.960	10
72.5	0.826	10
74.5	0.623	10
76.6	0.567	10
78.6	0.497	10
80.7	0.436	10
82.7	0.352	10
84.7	0.319	10
86.8	0.346	10
88.8	0.307	10
90.8	0.284	10
92.8	0.248	10
94.8	0.244	10
96.8	0.230	10
98.8	0.206	10
102.8	0.158	10
106.7	0.157	10
110.6	0.0985	10

TABLE VI. Differential cross sections for elastic scattering of 61.4 MeV protons on ^{27}Al.

$\theta_{c.m.}$ (deg)	$\sigma(\theta)$ (mb/sr)	±%
20.8	585	5
22.8	348	5
24.9	212	5
27.0	93.7	5
31.1	31.6	5
33.2	27.2	5
35.3	25.5	5
39.4	28.2	5
41.5	28.6	5
43.5	23.7	5
47.6	17.8	5
49.7	12.5	5
51.7	9.15	5
53.8	7.14	5
55.8	4.49	10
57.9	3.95	10
59.9	3.19	10
62.0	2.49	10
64.0	2.42	10
66.0	2.18	10
68.0	1.98	10
70.1	1.66	10
72.1	1.39	10
76.1	1.01	10
78.2	0.651	10
80.2	0.457	10
82.2	0.395	10
84.2	0.372	10
86.3	0.238	10
88.2	0.202	21
90.3	0.224	16
92.3	0.170	18
94.3	0.160	20
96.3	0.149	15
98.3	0.148	12
100.2	0.106	15
102.2	0.108	18
104.2	0.113	13
106.2	0.110	16
108.2	0.0848	15
110.2	0.0700	20
112.1	0.0615	20
114.1	0.0339	26

TABLE VII. Differential cross sections for elastic scattering of 61.4-MeV protons on ^{40}Ca.

$\theta_{c.m.}$ (deg)	$\sigma(\theta)$ (mb/sr)	±%
29.7	46.1	10
31.8	56.5	5
32.8	60.3	5
33.8	60.6	5
35.8	56.5	5
37.9	40.4	5
42.0	29.1	5
44.0	20.4	5
46.0	12.5	5
48.1	7.84	5
50.1	5.62	5
52.1	4.66	5
54.2	4.50	5
56.2	3.90	5
58.2	3.91	5
60.3	3.21	5
63.3	2.88	5
64.3	2.31	5
67.3	1.60	5
69.3	1.25	5
71.4	0.918	5
73.4	0.701	5
75.4	0.648	5
77.4	0.535	5
81.4	0.467	5
83.4	0.442	5
85.4	0.406	5
87.4	0.323	5
89.4	0.283	5
91.4	0.199	5
93.4	0.149	5
95.4	0.124	8
99.4	0.0686	10
103.4	0.0364	10
107.4	0.0415	10

TABLE VIII. Differential cross sections for elastic scattering of 61.4-MeV protons on ^{58}Ni.

$\theta_{c.m.}$ (deg)	$\sigma(\theta)$ (mb/sr)	±%
20.1	379	5
22.4	112	5
24.4	52.2	5
26.5	56.7	5
28.5	95.4	5
30.5	118	5
32.6	123	5
34.9	109	5
36.6	88.1	5
38.6	61.1	10
40.7	39.7	5
42.8	22.2	5
44.7	14.4	5
46.8	10.7	5
48.8	11.2	15
50.8	9.59	10
52.8	11.0	10
54.9	10.5	10
56.9	9.65	10
58.9	6.80	10
60.9	5.06	10
62.9	3.41	10
64.9	2.87	10
67.0	2.45	10
69.0	2.04	10
71.0	1.86	10
73.0	1.64	10
75.0	1.56	10
77.0	1.49	5
79.0	1.18	10
81.0	0.873	10
83.0	0.667	10
85.0	0.473	10
87.1	0.336	11
89.1	0.261	11
91.1	0.240	10
93.1	0.196	11
95.1	0.192	11
97.0	0.177	20
99.0	0.218	10
101.0	0.193	11
103.0	0.189	11
105.0	0.144	11
107.0	0.133	13
109.0	0.0919	16
111.0	0.0732	18
113.0	0.0607	19

TABLE IX. Differential cross sections for elastic scattering of 61.4-MeV protons on ^{68}Zn.

$\theta_{c.m.}$ (deg)	$\sigma(\theta)$ (mb/sr)	±%
17.2	838	5
19.3	304	5
21.3	82.6	5
23.3	49.2	5
25.4	113	5
27.3	135	5
29.4	172	5
31.4	140	5
33.5	119	5
35.5	72.6	5
37.5	47.6	5
39.5	22.4	5
41.6	15.4	5
43.6	12.3	5
45.6	12.8	5
47.6	14.1	5
49.6	14.7	5
51.7	12.2	5
53.7	10.1	5
55.7	7.39	5
57.7	4.91	5
59.7	3.11	5
61.7	2.51	5
63.8	2.25	5
66.8	2.12	5
68.8	1.99	5
70.8	1.76	5
72.1	1.69	5
74.8	1.51	5
76.8	1.02	5
78.8	0.787	5
80.8	0.481	8
82.8	0.449	8
86.8	0.271	8
88.8	0.287	8
90.8	0.324	8
92.8	0.261	8
94.8	0.236	8
98.8	0.193	8
102.8	0.106	8
106.8	0.0903	8

TABLE X. Differential cross sections for elastic scattering of 61.4-MeV protons on ^{90}Zr.

$\theta_{c.m.}$ (deg)	$\sigma(\theta)$ (mb/sr)	±%
20.2	82.4	5
22.3	94.5	5
24.3	208	5
26.3	289	5
28.3	330	5
30.3	247	5
32.4	175	5
34.4	94.5	5
36.4	46.3	5
38.4	18.0	5
40.4	17.9	5
42.5	23.8	10
44.5	31.6	5
46.5	21.9	10
48.5	29.4	5
50.5	19.1	10
52.5	13.5	10
54.5	8.10	10
56.6	5.65	10
58.6	4.04	10
60.6	4.29	5
62.6	4.82	10
64.6	4.86	10
66.6	4.61	10
68.6	3.87	10
70.6	2.65	10
72.6	1.78	10
74.7	1.39	10
76.7	0.940	12
78.7	1.106	10
80.7	0.916	10
82.7	0.820	11
84.7	0.947	10
86.7	0.768	13
88.7	0.722	11
90.7	0.450	11
92.7	0.322	11
94.7	0.246	13
96.7	0.185	15
98.7	0.143	13
100.7	0.161	16
102.7	0.169	14
104.7	0.188	14
106.7	0.197	12
108.6	0.0966	17
110.6	0.149	14
112.6	0.110	17

TABLE XI. Differential cross sections for elastic scattering of 61.4-MeV protons on ^{116}Sn.

$\theta_{c.m.}$ (deg)	$\sigma(\theta)$ (mb/sr)	±%
20.2	107	5
22.2	279	5
24.2	407	5
26.2	407	5
28.2	337	5
30.3	194	5
32.3	97.1	5
34.3	36.0	5
36.3	17.5	10
38.3	22.9	10
40.3	39.7	5
42.3	43.3	5
44.4	41.2	5
46.4	29.0	5
48.4	19.5	5
50.4	11.6	10
52.4	7.04	10
54.4	5.00	10
56.4	6.07	10
58.4	7.30	10
60.5	6.85	10
62.5	6.38	10
64.5	4.86	10
66.5	3.13	10
68.5	2.08	10
70.5	1.50	10
72.5	1.21	10
74.5	1.32	10
76.5	1.54	10
78.5	1.34	10
80.5	1.20	10
82.5	0.988	10
84.5	0.726	10
86.5	0.501	10
88.5	0.308	13
90.5	0.260	15
92.5	0.204	20
94.5	0.320	11
96.5	0.301	13
98.5	0.382	14
100.5	0.247	17
102.5	0.256	13
104.5	0.174	20
106.5	0.143	20
108.5	0.126	25
110.5	0.0543	30
112.5	0.0505	30

TABLE XII. Differential cross sections for elastic scattering of 61.4-MeV protons on ^{208}Pb.

$\theta_{c.m.}$ (deg)	$\sigma(\theta)$ (mb/sr)	±%
20.1	1581	5
22.1	1367	5
24.1	972	5
26.1	429	5
28.1	137	5
30.1	45.1	5
32.2	78.7	5
34.2	125	5
36.2	153	5
38.2	116	5
40.2	72.5	5
42.2	28.8	8
44.2	9.55	8
46.2	12.0	8
48.2	19.4	8
50.2	27.4	8
52.2	26.7	8
54.2	18.2	8
56.2	9.90	8
58.2	4.07	8
60.3	3.28	10
62.3	4.36	10
64.2	5.29	7
66.3	7.02	7
68.3	4.50	7
70.3	3.02	10
72.3	1.86	5
74.3	0.989	11
76.3	1.17	11
78.3	1.38	11
80.3	1.69	7
82.3	1.66	10
84.3	1.29	10
86.3	0.887	10
88.3	0.689	10
90.3	0.288	15
92.3	0.440	11
94.3	0.349	13
96.3	0.511	12
98.3	0.452	12
100.3	0.422	12
102.3	0.370	14
104.3	0.480	12
106.3	0.141	20
108.3	0.147	20
110.3	0.123	25
112.3	0.145	20